Exciton polaritons in a CuBr microcavity with HfO_2/SiO_2 distributed Bragg reflectors

M. Nakayama,* Y. Kanatanai, T. Kawase, and D. Kim

Department of Applied Physics, Graduate School of Engineering, Osaka City University, Sugimoto, Sumiyoshi-ku, Osaka 558-8585, Japan

(Received 16 March 2012; published 29 May 2012)

We have investigated the characteristics of exciton-photon strong coupling in a CuBr bulk microcavity that consists of a CuBr active layer with an effective thickness of $\lambda/2$ and HfO_2/SiO_2 distributed Bragg reflectors: λ corresponds to an effective resonant wavelength of the lowest-lying exciton. The CuBr crystal has three excitons labeled Z_f, $Z_{1,2}$, and Z_3 at the Γ point, where the Z_f exciton originates from a triplet state, which is peculiar to CuBr. Angle-resolved reflectance spectra measured at 10 K demonstrate the strong coupling behavior of the Z_f, $Z_{1,2}$, and Z_3 excitons and cavity photon, resulting in the formation of four cavity-polariton branches. Analyzing the cavity-polariton dispersion relations based on a phenomenological Hamiltonian for the strong coupling, we evaluated the vacuum Rabi-splitting energies of the Z_f, $Z_{1,2}$, and Z_3 excitons to be 31, 108, and 84 meV, respectively. These Rabi-splitting energies reflect the magnitudes of the oscillator strengths of the relevant excitons. Furthermore, we precisely measured angle-resolved photoluminescence (PL) spectra of the lower polariton branch under a weak excitation condition. In the bottleneck region, the population of the cavity polaritons is negligible, and the PL intensity at $k = 0$ is the highest. These facts suggest that the relaxation process of the cavity polaritons is not affected by a bottleneck effect.

DOI: 10.1103/PhysRevB.85.205320 PACS number(s): 78.66.Li, 71.36.+c, 71.35.−y, 78.40.Fy

I. INTRODUCTION

From the viewpoint of controlling exciton-photon interactions, semiconductor microcavities have attracted much attention in fundamental physics and applications.[1] In a microcavity, the excitons and cavity photon strongly couple each other, which leads to the formation of cavity polaritons. The strength of the strong coupling is characterized by the so-called vacuum Rabi-splitting energy, resulting from an anticrossing behavior between the dispersion relations of the exciton and cavity photon. Recently, wide-gap semiconductor microcavities including active layers of GaN (Refs. 2–7) or ZnO (Refs. 8–13) have been intensively investigated from the viewpoint of the stability of excitons. In Ref. 8, it was theoretically predicted that a ZnO-based microcavity is suitable for polariton lazing at room temperature. The main purpose of the investigations is to realize Bose–Einstein condensation of cavity polaritons[7] and polariton lasing.[4,5,13] Copper halides such as CuCl, CuBr, and CuI are also promising materials for wide-gap semiconductor microcavities: The exciton binding energies are 190, 108, and 62 meV for CuCl, CuBr, and CuI, respectively.[14] A considerable merit of copper halides is that crystalline thin films are easily prepared by a conventional vacuum deposition method.[15] We have fabricated CuCl (Refs. 16 and 17) and CuI (Ref. 18) microcavities and precisely analyzed the cavity-polariton dispersions. The typical values of the evaluated Rabi-splitting energies are ∼100 meV in CuCl microcavities[16,17] and ∼50 meV for CuI microcavities.[18] The excitonic properties of CuBr have a unique feature: The lowest energy exciton is a triplet state called the Z_f exciton. Thus, there exist three exciton states labeled Z_f, $Z_{1,2}$, and Z_3 at the Γ point in order of energy. The $Z_{1,2}$ (Z_3) exciton corresponds to the degenerate heavy-hole and light-hole excitons (the split-off-hole exciton). Note that the oscillator strength of the Z_f exciton is considerably enhanced by mixing between the singlet and triplet excitons.[19] Thus, a CuBr microcavity is a new type of a microcavity in the excitonic properties; however, there has been no report on cavity polaritons in a CuBr microcavity until now.

In this work, we have investigated the characteristics of cavity polaritons in a CuBr microcavity with HfO_2/SiO_2 distributed Bragg reflectors (DBRs). From angle-resolved reflectance spectra, we experimentally determined the dispersion relations of the cavity polaritons consisting of four branches due to the strong coupling between the Z_f, $Z_{1,2}$, and Z_3 excitons and cavity photon. On the basis of a phenomenological Hamiltonian, we analyzed the cavity polariton dispersions and evaluated the Rabi-splitting energies. Furthermore, we precisely measured angle-resolved photoluminescence (PL) spectra of the lower polariton branch (LPB) as an image map. We discuss the cavity-polariton dispersions and the relaxation process of the cavity polaritons.

II. EXPERIMENTAL DETAILS

The sample of a CuBr microcavity with HfO_2/SiO_2 DBRs was prepared on a (0001) Al_2O_3 substrate. The CuBr active layer with a thickness of $\lambda/2$ was sandwiched by the DBRs: The thickness of λ corresponds to an effective resonant wavelength of the lowest lying exciton. The bottom and top DBRs consisted of 9.5 and 8.5 periods, respectively, and each DBR was terminated by the HfO_2 layer. The HfO_2 and SiO_2 layers were fabricated by rf magnetron sputtering. Commercially supplied plates of HfO_2 with a purity of 99.9% and SiO_2 with a purity of 99.99% were used as the targets. The sputtering gas was Ar under a pressure of 1.33 Pa, and the substrate temperature was room temperature. Because CuBr is a hygroscopic material, the DBRs also acted as protective layers.[20] The CuBr active layer was grown at 60 °C by vacuum deposition using CuBr powders with a purity of 99.999% in 5×10^{-6} Pa. It was confirmed from X-ray diffraction patterns that the crystalline CuBr layer is just oriented along the [111] direction. Because the active layer thickness was $\lambda/2$, there was no spacer layer to form the cavity; namely, the sample belongs to the category of a bulk microcavity. The effective length, λ, is given by $\lambda_{EX}/\sqrt{\varepsilon_b}$ in a bulk microcavity,[21] where λ_{EX} is the resonant wavelength of the lowest lying exciton

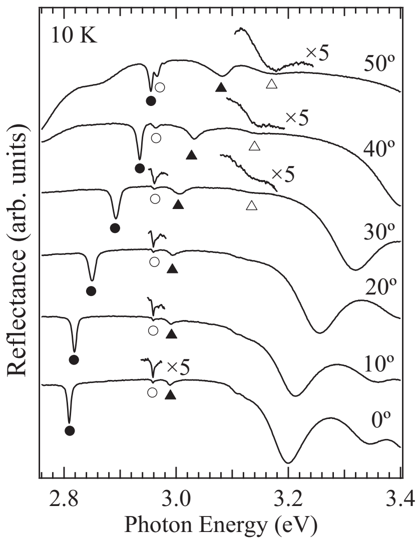

FIG. 1. Angle-resolved reflectance spectra of the $\lambda/2$-thick CuBr microcavity. The solid circles, open circles, solid triangles, and open triangles indicate the cavity-polariton modes.

in vacuum, and ε_b is the background dielectric constant. The length of $\lambda/2$ corresponds to 88 nm, where $\varepsilon_b = 5.7$ (Ref. 14), and the exciton energy is 2.963 eV, which is defined below from an absorption spectrum. In addition, a CuBr thin film with a thickness of 50 nm was prepared to observe an absorption spectrum. The growth rates of the CuBr, HfO_2, and SiO_2 layers were precisely monitored during the deposition process using a crystal oscillator.

In measurements of angle-resolved reflectance spectra, the probe light source was a Xe lamp, and the reflected light was detected with a charge-coupled device attached to a 32-cm single monochromator with a resolution of 0.15 nm. The p-polarized light was used in the reflectance measurement. An absorption spectrum was also measured to confirm the exciton energies and to estimate the relative oscillator strengths of the excitons with the use of the same system in the reflectance measurement. The excitation light for angle-resolved PL spectra was the 325-nm line of a He-Cd laser with a power density of $\sim$50 mW/cm^2. In the measurements of angle-resolved PL spectra, the incidence angle of the excitation light was fixed to 0°, whereas the detection angle was varied. The PL spectra were analyzed with the same monochromator system in the reflectance measurement. All of the optical measurements were performed at 10 K.

III. RESULTS AND DISCUSSION

Figure 1 shows the angle-resolved reflectance spectra of the CuBr microcavity. The four dips in the reflectance spectra are labeled with solid circles, open circles, solid triangles, and open triangles. The broad dip located at higher than $\sim$3.2 eV corresponds to a high–energy-side stop band of the DBR. As described above, CuBr has the Z_f, $Z_{1,2}$, and Z_3 excitons; therefore, four cavity polariton branches should exist under the strong coupling between the three excitons and cavity photon. The energies of the four reflectance dips labeled by the symbols systematically depend on the incidence angle. This fact indicates that the four reflectance dips are attributed to the cavity polaritons: the LPB, middle polariton branch 1 (MPB1), middle polariton branch 2 (MPB2), and upper polariton branch (UPB) in order of energy. We estimate the quality factor, Q, of the microcavity from the full width at half maximum of the reflectance dip of the LPB mode at the incidence angle of 0°: $Q = \sim 480$.

Next, we analyze the dispersion relations of the cavity polaritons. To analyze the experimental results of the incidence-angle dependence of the reflectance-dip energies, the eigenenergies of the cavity polaritons are calculated using the following phenomenological 4×4 Hamiltonian for the strong coupling between the Z_f, $Z_{1,2}$, and Z_3 excitons and cavity photon,

$$\begin{pmatrix} E_{\mathrm{cav}}(\theta) & \Omega_{Z(f)}/2 & \Omega_{Z(1,2)}/2 & \Omega_{Z(3)}/2 \\ \Omega_{Z(f)}/2 & E_{Z(f)} & 0 & 0 \\ \Omega_{Z(1,2)}/2 & 0 & E_{Z(1,2)} & 0 \\ \Omega_{Z(3)}/2 & 0 & 0 & E_{Z(3)} \end{pmatrix} \tag{1}$$

where $E_{Z(f)}$, $E_{Z(1,2)}$, and $E_{Z(3)}$ are the energies of the Z_f, $Z_{1,2}$, and Z_3 excitons, respectively, and $\Omega_{Z(f)}$, $\Omega_{Z(1,2)}$, and $\Omega_{Z(3)}$ are the vacuum Rabi-splitting energies of the relevant excitons that are fitting parameters. The energy of the cavity photon, $E_{\mathrm{cav}}(\theta)$, is given by[22]

$$E_{\mathrm{cav}}(\theta) = E_0 \left(1 - \frac{\sin^2\theta}{n_{\mathrm{eff}}^2}\right)^{-1/2}, \tag{2}$$

where θ, E_0, and n_{eff} are the incidence angle, energy of the cavity photon at $\theta = 0°$, and effective refractive index of the cavity, respectively. According to Ref. 23, we have to take into account the penetration of the light confined in the cavity into the DBR to calculate $E_{\mathrm{cav}}(\theta)$. Therefore, E_0 and n_{eff} are treated as fitting parameters. The Rabi-splitting energy is proportional to the square root of the excitonic oscillator strength.[6] So, if we have the information of the oscillator strengths of the three excitons in CuBr, the ambiguity of fitting the Rabi-splitting energies are considerably reduced. However, no data for oscillator strengths are available, except for the $Z_{1,2}$ exciton.

In this work, we estimate the relative oscillator strengths from the absorption spectrum of the CuBr thin film shown in Fig. 2, where the thin solid curve indicates the experimental result. We performed the line-shape analysis of the absorption spectrum using Gaussian functions for the exciton absorption bands that are shown by dashed curves. For the continuum states in the energy region higher than $\sim$3.08 eV, we used the following Sommerfeld factor:[24]

$$S \propto H(\Delta)\frac{\pi \exp(\pi/\sqrt{\Delta})}{\sinh(\pi/\sqrt{\Delta})} \tag{3}$$

with

$$\Delta = (\hbar\omega - E_g)/E_b, \tag{4}$$

where H is a unit step function, E_g is the band-gap energy, and E_b is the exciton binding energy. The thick solid curve indicates the total fitted results. The step-like edge at $\sim$3.08 eV results from the Sommerfeld factor. In the energy range from $\sim$2.99 to $\sim$3.08 eV, the fitted spectrum deviates from the experimental one. The reason for the deviation may be attributed to the neglect of excitons with $n \geqslant 2$ and various

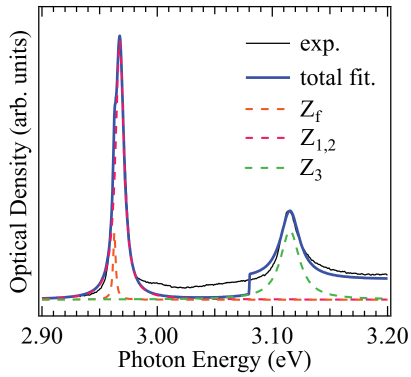

FIG. 2. (Color online) Absorption spectrum of the CuBr thin film, where thin solid curve indicates the experimental result. For the line-shape analysis, Gaussian functions are used for fitting the exciton absorption bands (dashed curves). For the continuum transitions, Eq.(3) is used. The thick solid curve indicates the total fitted results.

phonon-assisted bands. Note that the deviation hardly affects the estimation of the relative oscillator strengths. From the integrated intensities of the absorption bands of the Z_f, $Z_{1,2}$, and Z_3 excitons, we estimate the relative oscillator strengths as follows: $f_{Z(f)}$:$f_{Z(1,2)}$:$f_{Z(3)}$ = 0.083:1:0.61. The energies of the Z_f, $Z_{1,2}$, and Z_3 excitons are 2.963, 2.967, and 3.115 eV, respectively.

Figure 3 shows the incidence-angle dependence of the energies of the four cavity-polariton modes (LPB, MPB1, MPB2, and UPB), where the solid circles, open circles, solid triangles, and open triangles, which are the same symbols in Fig. 1, indicate the experimental results. The solid curves depict the fitted results using Eq. (1). The dashed horizontal lines indicate the exciton energies, and the dashed curve shows the cavity-photon dispersion. The values of E_0 and n_{eff} in Eq. (2) are 2.835 eV and 1.85, respectively. Because the background refractive index of CuBr is $\sqrt{\varepsilon_b} = 2.4$, the smaller value of n_{eff} reflects penetration of the light confined in the cavity into the DBR. It is evident that the fitted results well explain the experimental results. Thus, we have succeeded in analyzing the four cavity polariton branches. The Rabi-splitting energies are evaluated as 31, 108, and 84 meV for the Z_f, $Z_{1,2}$, and Z_3 excitons, respectively. The error of the evaluation is $\pm 7\%$. Here, we compare the Rabi-splitting energies with those of other semiconductor microcavities. Because the Rabi-splitting energy markedly depends on the active layer thickness,[17] the thicknesses should be the same for comparison. In a $\lambda/2$-thick ZnO microcavity with HfO_2/SiO_2 DBRs, the Rabi-splitting energy of the A exciton was reported as 30 meV.[11] As described above, Rabi-splitting energy is proportional to the square root of the excitonic oscillator strength. The oscillator strength is given by $f = \varepsilon_b(E_L^2 - E_T^2)$, where E_L (E_T) is a longitudinal (transverse) exciton energy.[25] The oscillator strengths of the $Z_{1,2}$ exciton in CuBr and the A exciton in ZnO are 4.2×10^5 (Ref. 14) and 4.9×10^4 meV^2 (Ref. 11), respectively. Therefore, the ratio of the Rabi-splitting energy of the A exciton to that of the $Z_{1,2}$ exciton is expected to be $\Omega_A : \Omega_{Z(1,2)} = \sqrt{f_A} : \sqrt{f_{Z(1,2)}} = 1 : 2.9$. The experimental ratio, 1:3.6, deviates from the expected ratio by 24%. The difference between the expected and experimental ratios might be from some uncertainty of the values of E_L and E_T.

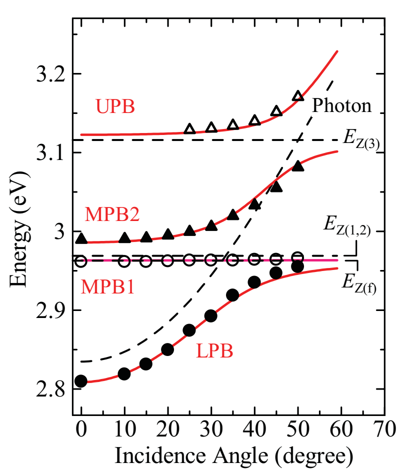

FIG. 3. (Color online) Incidence-angle dependence of the energies of the four cavity-polariton modes in the $\lambda/2$-thick CuBr microcavity, where the solid circles, open circles, solid triangles, and open triangles, which are the same symbols in Fig. 1, indicate the experimental results. The solid curves depict the fitted results with Eq. (1). The dashed horizontal lines indicate the exciton energies, and the dashed curve shows the cavity-photon dispersion.

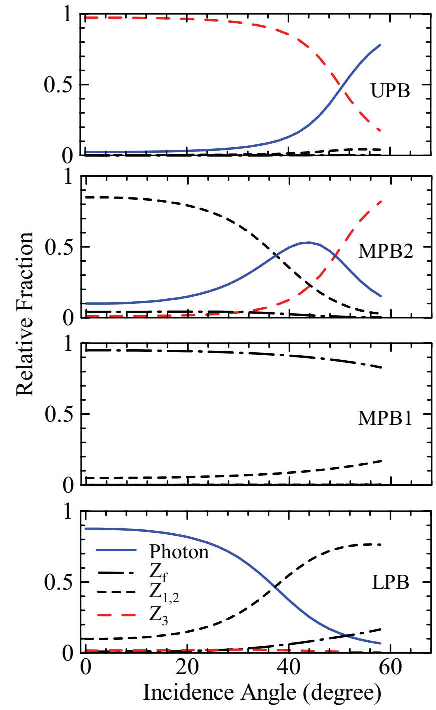

FIG. 4. (Color online) Relative fractions of the Z_f, $Z_{1,2}$, and Z_3 excitons and cavity photon in the LPB, MPB1, MPB2, and UPB modes as a function of incidence angle. The relative fractions correspond to the eigenvectors of Eq. (1).

Figure 4 show the relative fractions of the Z_f, $Z_{1,2}$, and Z_3 excitons and cavity photon in the LPB, MPB1, MPB2, and UPB modes as a function of incidence angle. The relative fractions correspond to the eigenvectors of Eq. (1). In the LPB mode, the cavity photon is the major fraction in the angle region lower than $\sim 36^\circ$, whereas the $Z_{1,2}$ exciton is the major fraction in the higher angle region. The Z_f exciton fraction, which is

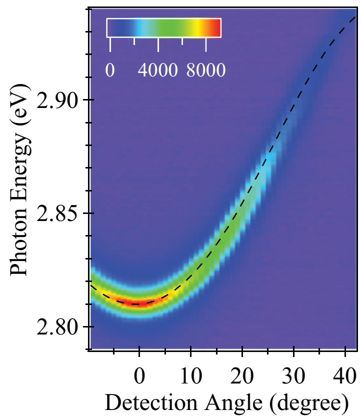

FIG. 5. (Color online) Angle-resolved PL spectra summarized as a color image map in the $\lambda/2$-thick CuBr microcavity, where the color scale intensity is depicted on the top. The dashed curve indicates the dispersion of the LPB.

the lowest energy exciton, is minor because of the smaller oscillator strength. The MPB1 mode has no cavity-photon fraction. This results in the fact that the dispersion of the MPB1 is flat, as shown in Fig. 3. In the MPB2 mode, the $Z_{1,2}$ exciton fraction is the major fraction in the angle region lower than $\sim 36^\circ$. The fraction of the cavity photon reaches a peak at $\sim 44^\circ$. In the higher angle region, the major fraction is that of the Z_3 exciton. In the UPB mode, the Z_3 exciton fraction is the major fraction in the angle region lower than $\sim 50^\circ$, whereas the cavity-photon fraction is major in the higher angle region. The above-mentioned behaviors of the fractions of the Z_f, $Z_{1,2}$, and Z_3 excitons and the cavity photon explain the characteristics of the cavity polaritons.

Finally, we discuss the angle-resolved PL spectra, summarized as a color image map shown in Fig. 5, in which the dashed curve indicates the LPB dispersion. It is evident that the PL originates from the LPB mode. The PL intensity gradually increases with a decrease in detection angle lower than $\sim 30^\circ$: The PL intensity is the highest at 0°, corresponding to the in-plane wave vector $k = 0$. Tartakovskii *et al.*[26] reported that a relaxation bottleneck of cavity polaritons exists in a GaAs microcavity and that the bottleneck effect is suppressed by an increase in excitation power density from 5 to 80 W/cm^2 owing to exciton-exciton scattering processes. In the present case, the bottleneck region of the LPB is around 35° from Fig. 3; however, the population of the cavity polaritons in the bottleneck region is negligible, as shown in Fig. 5. Note that the excitation power density is very weak: $\sim 50\ mW/cm^2$. Thus, in the CuBr microcavity, the relaxation process of the cavity polaritons is not affected by the bottleneck effect. The reason why there is no bottleneck effect is considered to be as follows. In this case, exciton-exciton and/or polariton-polariton scattering processes do not contribute to the relaxation process because of the very weak excitation power density. Because CuBr has high ionicity, the interaction between the exciton and longitudinal optical (LO) phonon with an energy of 20.7 meV (Ref. 14) is strong.[27] Therefore, the LO-phonon scattering dominates the relaxation process. The lack of a bottleneck effect is advantageous for Bose–Einstein condensation of the cavity polaritons and polariton lasing. An investigation of polariton lasing in the CuBr microcavity is in progress, which will be reported elsewhere.

IV. CONCLUSIONS

We have fabricated the $\lambda/2$-thick CuBr microcavity with HfO_2/SiO_2 DBRs and experimentally determined the cavity-polariton dispersions using angle-resolved reflectance spectroscopy. Strong coupling between the Z_f, $Z_{1,2}$, and Z_3 excitons and cavity photon in the CuBr microcavity leads to the formation of four cavity-polariton branches. From the analysis of the cavity-polariton dispersions with the phenomenological Hamiltonian for the strong coupling, the vacuum Rabi-splitting energies for the Z_f, $Z_{1,2}$, and Z_3 excitons were evaluated as 31, 108, and 84 meV, respectively. The experimental cavity-polariton dispersions were well reproduced by the fitting procedure. We also calculated the relative fractions of the constituents to characterize the four cavity-polariton branches. Furthermore, the angle-resolved PL spectra were precisely measured. It was found that the PL intensity of the LPB mode gradually increases with a decrease in the detection angle: The PL intensity is the highest at 0°, corresponding to $k = 0$. We confirmed that the population of the cavity polaritons in the bottleneck region is negligible. These facts demonstrate that the relaxation process of the cavity polaritons is not affected by the bottleneck effect. This is advantageous for Bose–Einstein condensation of the cavity polaritons and polariton lasing.

ACKNOWLEDGMENTS

This work was supported by a Grant-in-Aid for Scientific Research (B) (No. 22340084) from the Japan Society for the Promotion of Science.

*nakayama@a-phys.eng.osaka-cu.ac.jp

[1] For a review, A. V. Kavokin, J. J. Baumberg, G. Malpuech, and F. P. Laussy, *Microcavities* (Oxford University Press, Oxford, 2007).

[2] N. Antoine-Vincent, F. Natali, D. Byrne, A. Vasson, P. Disseix, J. Leymarie, M. Leroux, F. Semond, and J. Massies, Phys. Rev. B **68**, 153313 (2003).

[3] I. R. Sellers, F. Semond, M. Leroux, J. Massies, M. Zamfirescu, F. Stokker-Cheregi, M. Gurioli, A. Vinattieri, M. Colocci, A. Tahraoui, and A. A. Khalifa, Phys. Rev. B **74**, 193308 (2006).

[4] S. Christopoulos, G. Baldassarri Höger von Högersthal, A. J. D. Grundy, P. G. Lagoudakis, A. V. Kavokin, J. J. Baumberg, G. Christmann, R. Butté, E. Feltin, J.-F. Carlin, and N. Grandjean, Phys. Rev. Lett. **98**, 126405 (2007).

[5] G. Christmann, R. Butté, E. Feltin, J.-F. Carlin, and N. Grandjean, Appl. Phys. Lett. **93**, 051102 (2008).

[6] F. Réveret, P. Disseix, J. Leymarie, A. Vasson, F. Semond, M. Leroux, and J. Massies, Phys. Rev. B **77**, 195303 (2008).

[7] J. Levrat, R. Butté, E. Feltin, J.-F. Carlin, N. Grandjean, D. Solnyshkov, and G. Malpuech, Phys. Rev. B **81**, 125305 (2010).

[8] M. Zamfirescu, A. Kavokin, B. Gil, G. Malpuech, and M. Kaliteevski, Phys. Rev. B **65**, 161205(R) (2002).
[9] R. Shimada, J. Xie, V. Avrutin, Ü. Özgür, and H. Morkoç, Appl. Phys. Lett. **92**, 011127 (2008).
[10] M. Nakayama, S. Komura, T. Kawase, and D. Kim, J. Phys. Soc. Jpn. **77**, 093705 (2008).
[11] T. Kawase, D. Kim, K. Miyazaki, and M. Nakayama, Phys. Status Solidi B **248**, 460 (2011).
[12] F. Médard, J. Zuniga-Perez, P. Disseix, M. Mihailovic, J. Leymarie, A. Vasson, F. Semond, E. Frayssinet, J. C. Moreno, M. Leroux, S. Faure, and T. Guillet, Phys. Rev. B **79**, 125302 (2009).
[13] T. Guillet, M. Mexis, J. Levrat, G. Rossbach, C. Brimont, T. Bretagnon, B. Gil, R. Butté, N. Grandjean, L. Orosz, F. Réveret, J. Leymarie, J. Zuniga-Pérez, M. Leroux, F. Semond, and S. Bouchoule, Appl. Phys. Lett. **99**, 161104 (2011).
[14] M. Ueta, H. Kanzaki, K. Kobayashi, Y. Toyozawa, and E. Hanamura, *Excitonic Processes in Solids* (Springer, New York, 1986), p. 116.
[15] M. Nakayama, A. Soumura, K. Hamasaki, H. Takeuchi, and H. Nishimura, Phys. Rev. B **55**, 10099 (1997).
[16] G. Oohata, T. Nishioka, D. Kim, H. Ishihara, and M. Nakayama, Phys. Rev. B **78**, 233304 (2008).
[17] M. Nakayama, K. Miyazaki, T. Kawase, and D. Kim, Phys. Rev. B **83**, 075318 (2011).
[18] M. Nakayama, M. Kameda, T. Kawase, and D. Kim, Phys. Rev. B **83**, 235325 (2011).
[19] S. Suga, K. Cho, and M. Bettini, Phys. Rev. B **13**, 943 (1976).
[20] K. Miyazaki, D. Kim, T. Kawase, M. Kameda, and M. Nakayama, Jpn. J. Appl. Phys. **49**, 042802 (2010).
[21] Y. Chen, A. Tredicucci, and F. Bassani, Phys. Rev. B **52**, 1800 (1995).
[22] M. S. Skolnick, T. A. Fisher, and D. M. Whittaker, Semicond. Sci. Technol. **13**, 645 (1998).
[23] G. Panzarini, L. C. Andreani, A. Armitage, D. Baxter, M. S. Skolnick, V. N. Astratov, J. S. Roberts, A. V. Kavokin, M. R. Vladimirova, and M. A. Kaliteevski, Phys. Rev. B **59**, 5082 (1999).
[24] H. Haug and S. W. Koch, *Quantum Theory of the Optical and Electronic Properties of Semiconductors* (World Scientific, Singapore, 1993), p. 169.
[25] C. F. Kingshirn, *Semiconductor Optics*, 3rd ed. (Springer, Berlin, 2007), p. 73.
[26] A. I. Tartakovskii, M. Emam-Ismail, R. M. Stevenson, M. S. Skolnick, V. N. Astratov, D. M. Whittaker, J. J. Baumberg, and J. S. Roberts, Phys. Rev. B **62**, R2283 (2000).
[27] J. Valenta, J. Moniatte, P. Gilliot, B. Hönerlage, J. B. Grun, R. Levy, and A. I. Ekimov, Phys. Rev. B **57**, 1774 (1998).